# Electronic Supplementary Information (ESI)

## Exploring structure, temperature and activity correlations in the selective oxidation of lower olefins over Bi-Mo-Co-Fe-O catalysts by spatial reactor profile measurements

Linda Klag,[a] Sebastian Weber,[a,b] Raimund Horn[c], Thomas L. Sheppard[a,b,†], Jan-Dierk Grunwaldt[a,b,*]

[a]Institute for Chemical Technology and Polymer Chemistry (ITCP), Karlsruhe Institute of Technology (KIT), 76131 Karlsruhe, Germany.

[b]Institute of Catalysis Research and Technology (IKFT), Karlsruhe Institute of Technology (KIT), 76344 Eggenstein-Leopoldshafen, Germany.

[c]Institute of Chemical Reaction Engineering, Hamburg University of Technology, 21073 Hamburg, Germany.

[†]Current address: Institute of Chemical Technology, Leipzig University, 04103 Leipzig, Germany.

*Corresponding author: grunwaldt@kit.edu

# 1 Setup for spatially-resolved catalytic testing

The setup for the spatially-resolved tests can roughly be divided in three main sections: (i) feed dosage, (ii) compact profile reactor (CPR) and (iii) on-line analytics. Sections (i) and (iii) correspond to a lab-scale testing unit for integral catalytic performance tests, which is described in detail elsewhere.(1, 2)

i) Feed dosage: The gases nitrogen (N50, Air Liquide), oxygen (N48, Air Liquide), propylene (N25, Air Liquide) and isobutene (N25, Air Liquide) were supplied by mass flow controllers (Bronkhorst), and water was dosed through a CEM (Bronkhorst). Educts and product species were transferred through the setup *via* heated lines (200 °C) to prevent product condensation.

ii) CPR: The CPR setup includes a fused silica reactor (outer diameter 6 mm, inner diameter 3.5 mm, length 180 mm), which was connected to the feed dosage and mounted in a vertically adjusted, motorised heating block (oven). A stainless-steel capillary (outer diameter 800 µm, inner diameter 520 µm, length 34 cm) with side-sampling orifices (4 x 50 µm) was placed through the centre of the reactor tube for local gas sampling. A thermocouple (type-K, outer diameter 250 µm) was inserted into the sampling capillary, with the tip aligned to the orifice position, for simultaneous temperature profiling. For each measurement, the sampling capillary was fixed at both ends of the CPR, while the reactor/ oven unit was moved along the capillary. In addition, the CPR casing and heating block/ oven exhibit a slot for *e.g.*, the X-ray beam to penetrate through the catalyst bed.

iii) On-line analytics: The integral product stream was monitored by an on-line oxygen sensor (PAROX 1200 H, MBE AG) to ensure the oxygen concentration and thus conversion remained constant during profile acquisition. The local product gas mixture was continuously extracted through the orifices and analysed by on-line gas chromatography (Agilent 7890B) and mass spectrometry (OMNI Star GSD 320, Pfeiffer Vacuum). The GC was equipped with two micro packed Hayesep Q columns ($CO_2$ retention), a micro packed molsieve 5 Å column for separation of other inorganic species ($N_2$, $O_2$, CO) and an HP-FFAP column for separation of organic species. The inorganic compounds were quantified by a thermal conductivity detector (TCD), while organic compounds were detected by a flame ionization detector (FID). Quantification of the detected peak areas was achieved by means of defined calibration gas mixtures giving a conversion factor for each substance in µmol per area unit.

# 2 Calculations

## 2.1 Conversion, selectivity and WHSV

Olefin (*i.e.*, propylene, isobutene) conversion was calculated according to equation (1):

$$X_{olefin}=\frac{n_{olefin}^{bypass}-n_{olefin}}{n_{olefin}^{bypass}} \quad \textbf{(1)}$$

Selectivity for the main products acrolein, acrylic acid, methacrolein, CO and $CO_2$ was calculated according to equations (2)-(9), considering the carbon atom number of each species. Acrolein and acrylic acid are relevant for selective propylene oxidation, methacrolein for selective isobutene oxidation and $CO_x$ for both reactions.

$$S_{acrolein}=\frac{3\cdot n_{acrolein}}{n_{CO}+n_{CO_2}+3\cdot n_{acrolein}+3\cdot n_{acrylic\ acid}} \quad \textbf{(2)}$$

$$S_{acrylic\ acid}=\frac{3\cdot n_{acrylic\ acid}}{n_{CO}+n_{CO_2}+3\cdot n_{acrolein}+3\cdot n_{acrylic\ acid}} \quad \textbf{(3)}$$

$$S_{CO}=\frac{n_{CO}}{n_{CO}+n_{CO_2}+3\cdot n_{acrolein}+3\cdot n_{acrylic\ acid}} \quad \textbf{(4)}$$

$$S_{CO_2}=\frac{n_{CO_2}}{n_{CO}+n_{CO_2}+3\cdot n_{acrolein}+3\cdot n_{acrylic\ acid}} \quad \textbf{(5)}$$

$$S_{methacrolein}=\frac{4\cdot n_{methacrolein}}{n_{CO}+n_{CO_2}+4\cdot n_{methacrolein}} \quad \textbf{(6)}$$

$$S_{CO}=\frac{n_{CO}}{n_{CO}+n_{CO_2}+4\cdot n_{methacrolein}} \quad \textbf{(7)}$$

$$S_{CO_2}=\frac{n_{CO_2}}{n_{CO}+n_{CO_2}+4\cdot n_{methacrolein}} \quad \textbf{(8)}$$

$$S_{CO_x}=S_{CO}+S_{CO_2} \quad \textbf{(9)}$$

The GHSV was calculated according to equation (10):

$$GHSV=\frac{\dot{V}_{in}}{V_{catalyst\ bed}} \quad \textbf{(10)}$$

## 2.2 Local formation/reaction rates

First, the total volume flow was converted to total molar flow assuming ideal gas conditions. The obtained value was multiplied with the individual concentration of each species measured by GC along the reactor. In this way, molar flow rates along the reactor were obtained. The first derivative of these molar flow rates was calculated, representing the local formation/ reaction rate.

# 3 Additional information on XRD analysis

## 3.1 Phase assignment by XRD

**Table S1**: List of main XRD reflections at λ = 0.12224 Å for relevant metal oxide phases of the Bi-Mo-Co-Fe-O system referenced in the ISCD database.

| Phase | Main reflection / ° | ICSD collection code |
|---|---|---|
| $\alpha$-$CoMoO_4$ | 2.26 | 23808(3) |
| $\beta$-$CoMoO_4$ | 2.08 | 760022(4) |
| $\beta$-$Co_{0.7}Fe_{0.3}MoO_4$ | 2.10 | 280035(5) |
| $Co_3O_4$ | 2.93 | 36256(6) |
| $\alpha$-$Bi_2Mo_3O_{12}$ | 2.23 | 2650(7) |
| $\beta$-$Bi_2Mo_2O_9$ | 2.21 | 201742(8) |
| $\gamma$-$Bi_2MoO_6$ | 2.25 | 17070(9) |
| $Bi_2O_3$ | 2.17 | 15072(10) |
| $\alpha$-$FeMoO_4$ | 2.24 | 43012(11) |
| $\beta$-$FeMoO_4$ | 2.08 | 43013(11) |
| $Fe_2Mo_3O_{12}$ | 1.82 | 16402(12) |
| $Fe_3O_4$ | 2.81 | 26410(13) |
| $Bi_3FeMo_2O_{12}$ | 2.25 | 45(14) |
| $MoO_3$ | 2.17 | 152312(15) |
| $Mo_{18}O_{52}$ | 1.98 | 27510(16) |

## 3.2 Rietveld refinement

Rietveld refinement was performed using TOPAS (v.6, Bruker AXS).(17) The spatially-resolved XRD patterns were first analysed with the references available from ICSD (**see Table S1**). Subsequently, corresponding crystallographic information files (CIFs) were downloaded from ICSD and used as initial structure models for the Rietveld refinement. A $LaB_6$ standard available at the P21.1 beamline (DESY, Hamburg, Germany) was used to derive an instrumental profile function (IPF). The IPF was described by a pseudo-Voigt Thompson-Cox-Hastings peak shape with refined *u*, *v*, *w*, and *x* parameters. The final refined $LaB_6$ parameters were used as fixed values for Rietveld refinement of sample data using the same peak shape description. For each structure, lattice parameters, scale factor, and the crystallite size related

profile broadening according to the double-Voigt approach by Balzar(18) were refined. Atomic parameters were kept fixed to literature reported values. The errors of the sequential refinement are given as error bars in the corresponding figures in the main article.

# 4 Additional activity and temperature profiles

## 4.1 Activity profiling during selective propylene oxidation

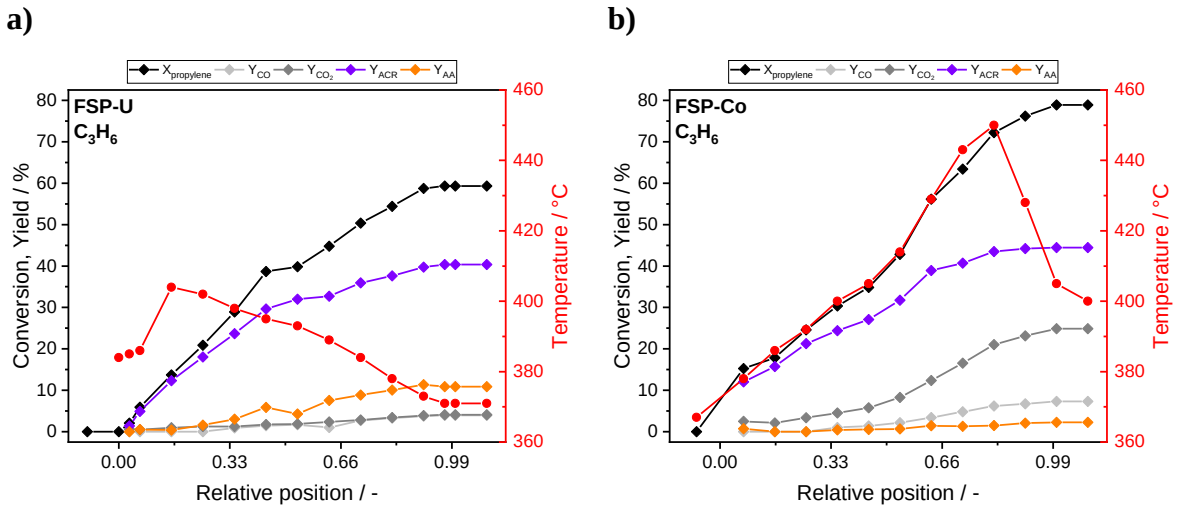


**Figure S1:** Propylene conversion and yield for each product species along the catalyst bed of FSP-U (a) and FSP-Co (b). Profiles were acquired under reaction conditions ($N_2/O_2/C_3H_6/H_2O$ = 70/14/8/8 vol%; GHSV 10877 $h^{-1}$) at 380 °C.

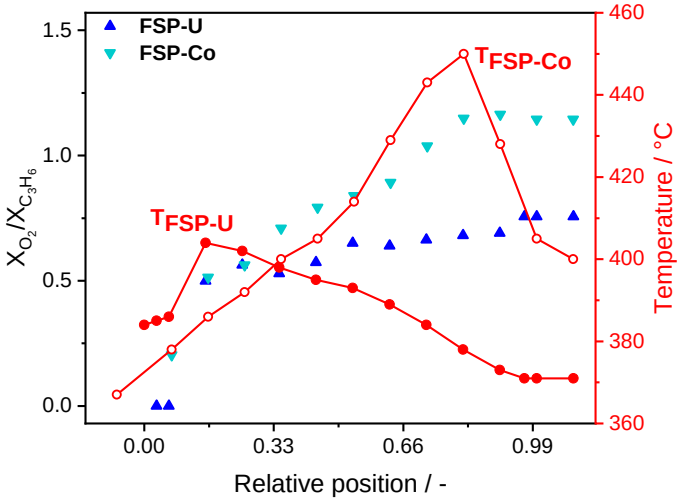


**Figure S2:** Oxygen to propylene conversion ratio of FSP-Co (light) and FSP-U (dark) together with temperature profiles along the catalyst bed during selective propylene oxidation.

## 4.2 Activity profiling during selective isobutene oxidation

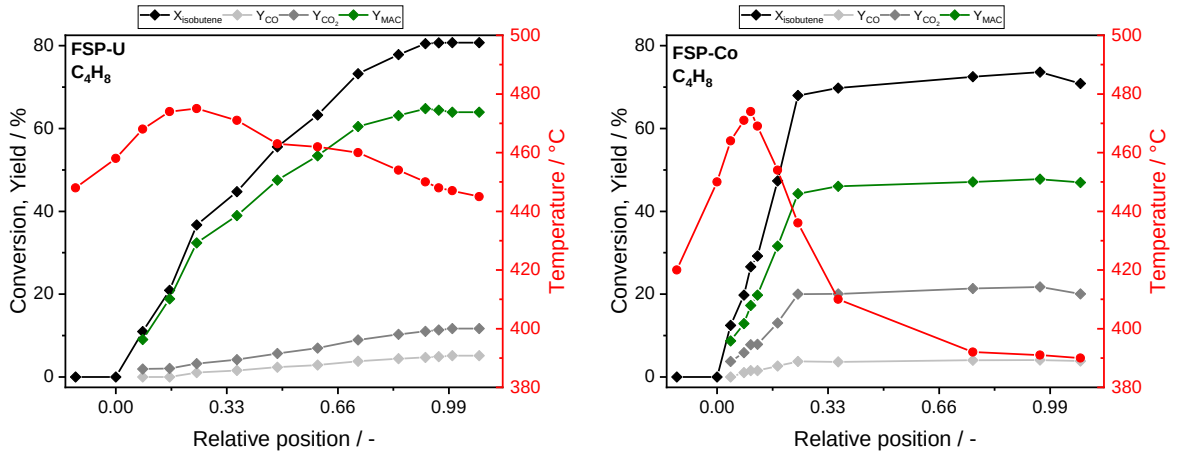


**Figure S3:** Isobutene conversion and yield for each product species along the catalyst bed of FSP-U (a) and FSP-Co (b). Profiles were acquired under reaction conditions ($N_2/O_2/C_4H_8/H_2O$ = 70/14/8/8 vol%; GHSV 12473 $h^{-1}$) at 450 °C (FSP-U) and 400 °C (FSP-Co) and catalysts were diluted with SiC (1:3).

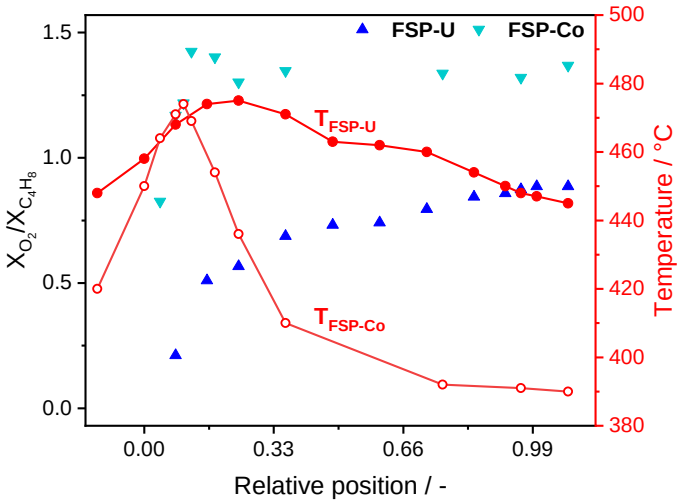


**Figure S4:** Oxygen to isobutene conversion ratio of FSP-Co (light) and FSP-U (dark) together with temperature profiles along the catalyst bed during selective isobutene oxidation.

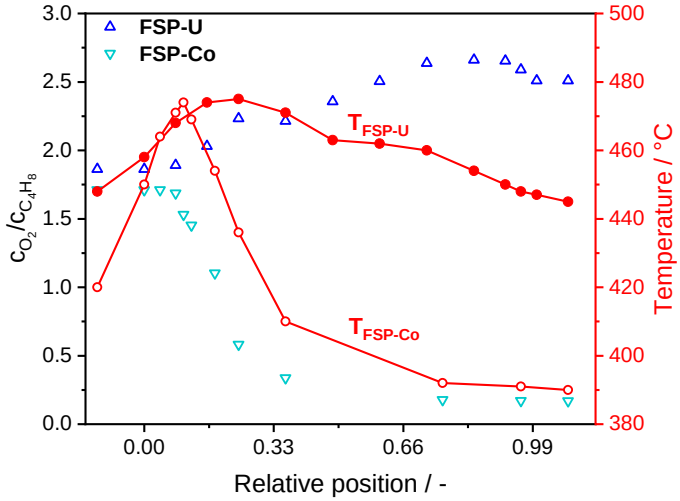


**Figure S5:** Molar ratio of oxygen to isobutene for FSP-Co (light) and FSP-U (dark) together with temperature profiles along the catalyst bed during selective isobutene oxidation.

## 4.3 Activity profiling during selective olefin oxidation

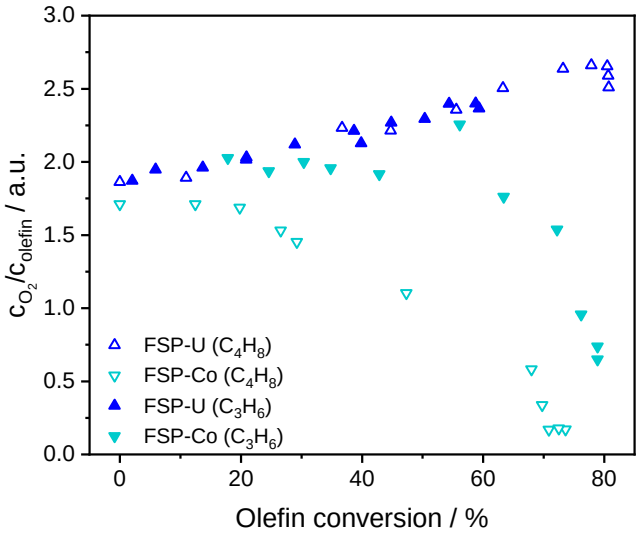


**Figure S6:** Molar ratio of oxygen/olefin over olefin conversion of FSP-Co (light) and FSP-U (dark) during selective propylene or isobutene oxidation.

# 5 Additional XRD data

## 5.1 Additional XRD profiles

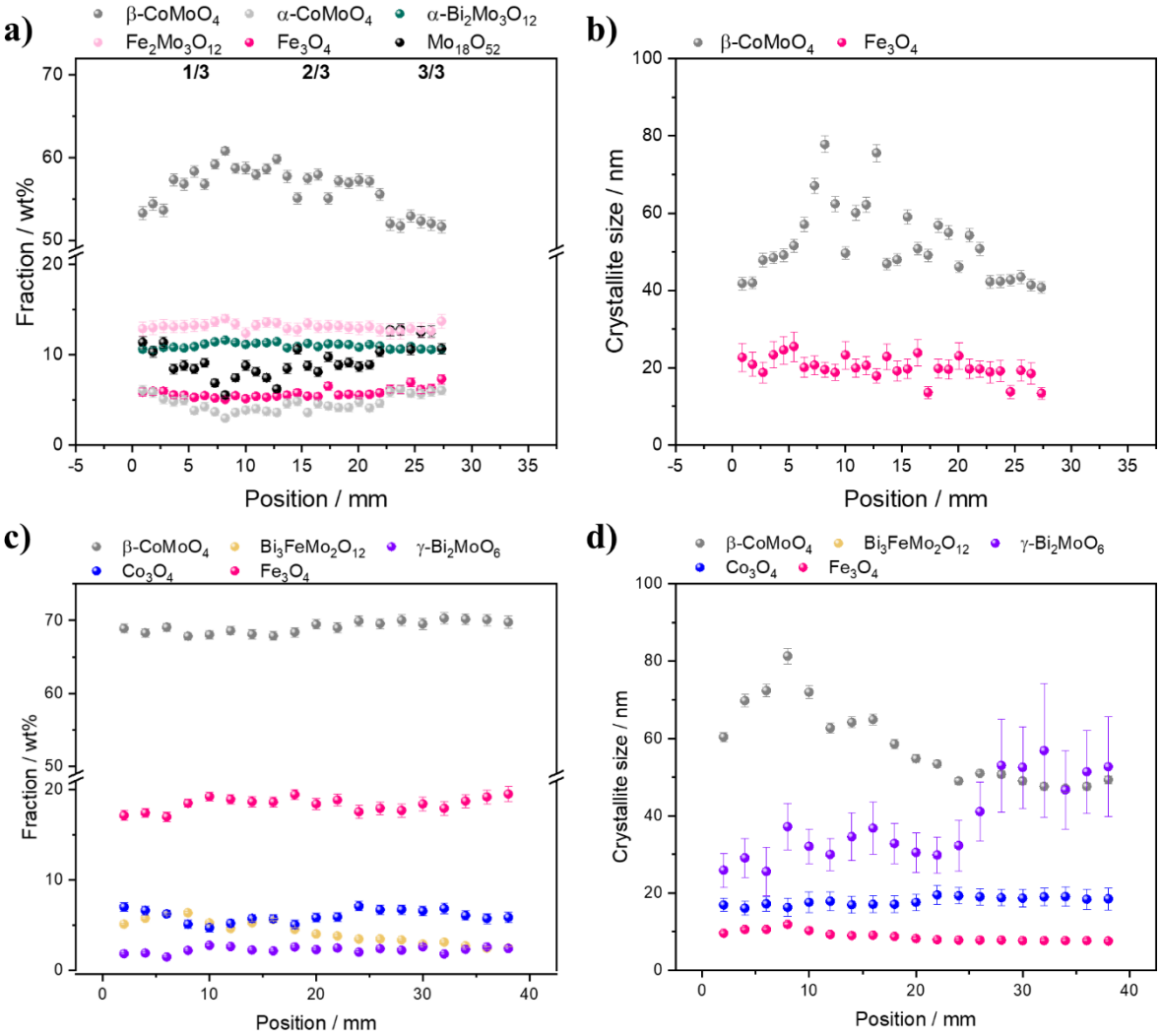


**Figure S7**: Non-averaged *ex situ* XRD results of FSP-U (a,b) and FSP-Co (c,d) showing distribution of crystalline phases and crystallite sizes derived from Rietveld refinement over the relative catalyst bed position.

**a)** **b)**

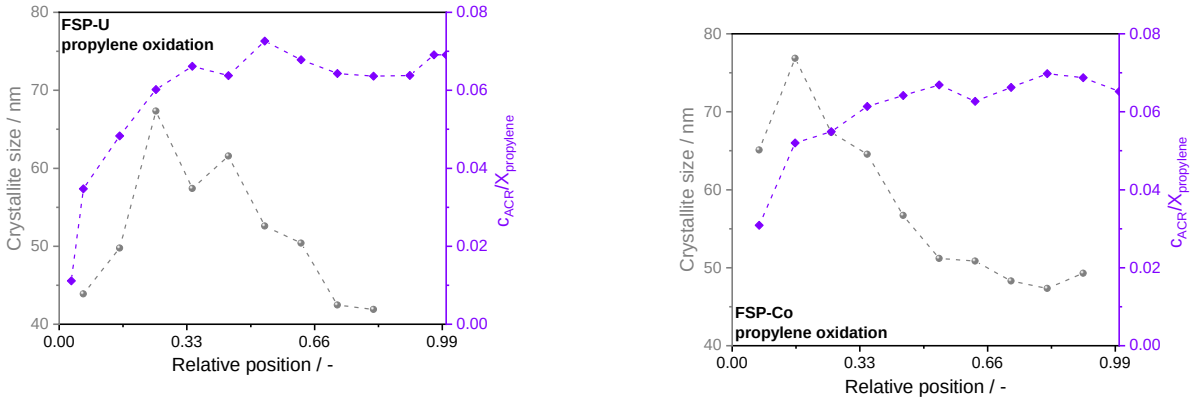


**Figure S8**: Crystallite size of $\beta$-$CoMoO_4$/ $\beta$-$Co_{0.7}Fe_{0.3}MoO_4$ and acrolein concentration over propylene conversion of FSP-U (a) and FSP-Co (b) plotted over the relative catalyst bed position.

## 5.2 Rietveld refinement results

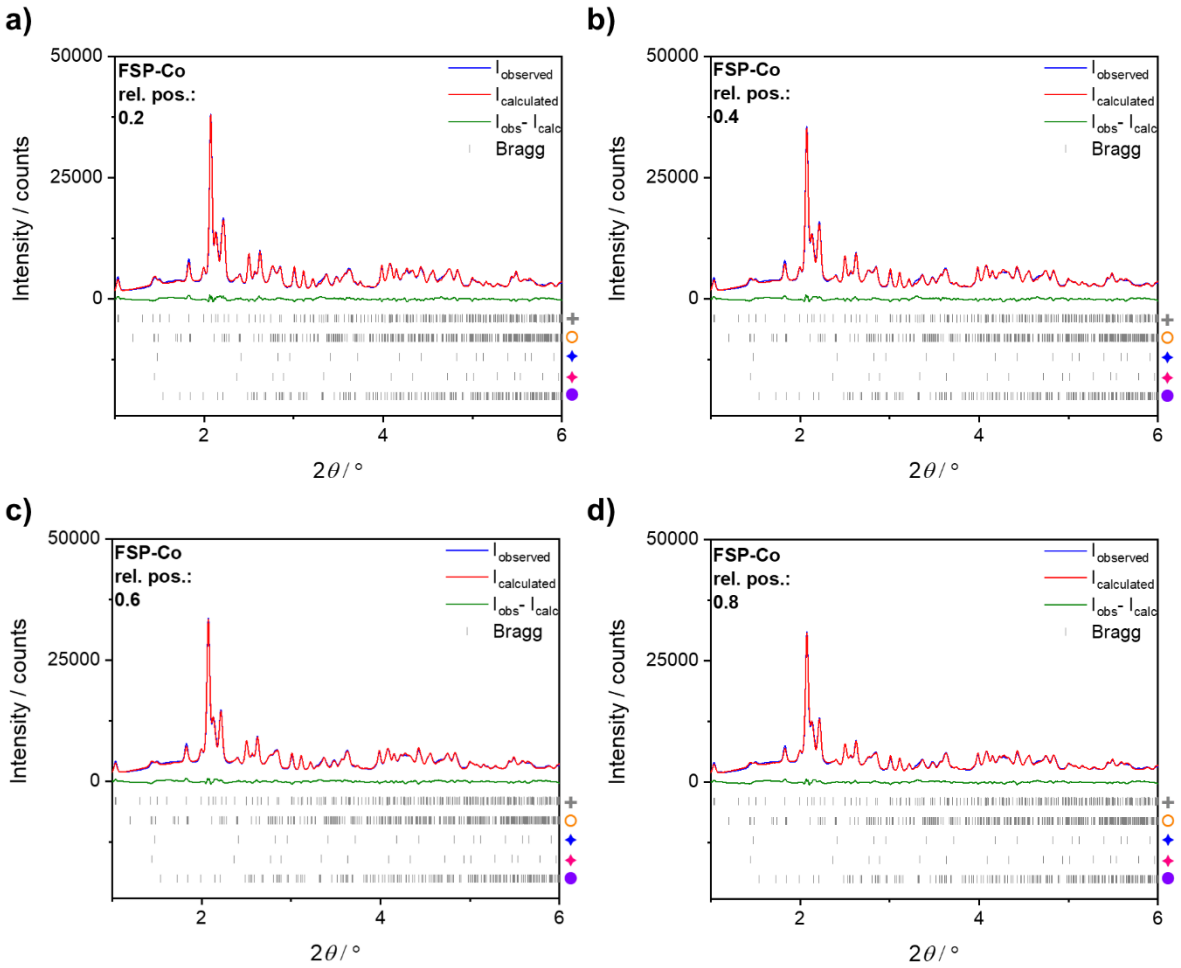


**Figure S9**: Selected Rietveld refinements of FSP-Co acquired at different positions along the catalyst bed, referring to relative position 0.2 (a), 0.4 (b), 0.6 (c) and 0.8 (d). Bragg markers refer top down to: $\beta$-$CoMoO_4$ (✚), $Bi_3FeMo_2O_{12}$ (○), $Co_3O_4$ (✦), $Fe_3O_4$ (✦) and $\gamma$-$Bi_2MoO_6$ (●). Fit results are listed in Table S2.

**Table S2:** Selected Rietveld refinements results of FSP-Co measured at different positions along the catalyst bed.

| **Results from Rietveld refinement** | **Relative position** | | | |
|---|---|---|---|---|
| | **0.2** | **0.4** | **0.6** | **0.8** |
| ω ($\beta$-$CoMoO_4$) / wt% | 68.3 (5) | 68.9 (6) | 70 (7) | 70 (7) |
| ω ($\gamma$-$Bi_2MoO_6$) / wt% | 2.2 (1) | 2.5 (1) | 2.4 (1) | 2.3 (1) |
| ω ($Co_3O_4$) / wt% | 4.9 (4) | 4.9 (4) | 6.4 (5) | 5.9 (5) |
| ω ($Fe_3O_4$) / wt% | 18.4 (5) | 19.1 (6) | 17.8 (7) | 18.5 (7) |
| ω ($Bi_3FeMo_2O_{12}$) / wt% | 6.3 (1) | 4.5 (1) | 3.4 (1) | 2.7 (1) |
| $R_{exp}$ / % | 1.50 | 1.50 | 1.50 | 1.53 |
| $R_{wp}$ / % | 4.35 | 4.35 | 3.86 | 4.05 |
| $R_p$ / % | 3.43 | 3.42 | 3.07 | 3.21 |
| GOF / % | 2.91 | 2.90 | 2.57 | 2.65 |

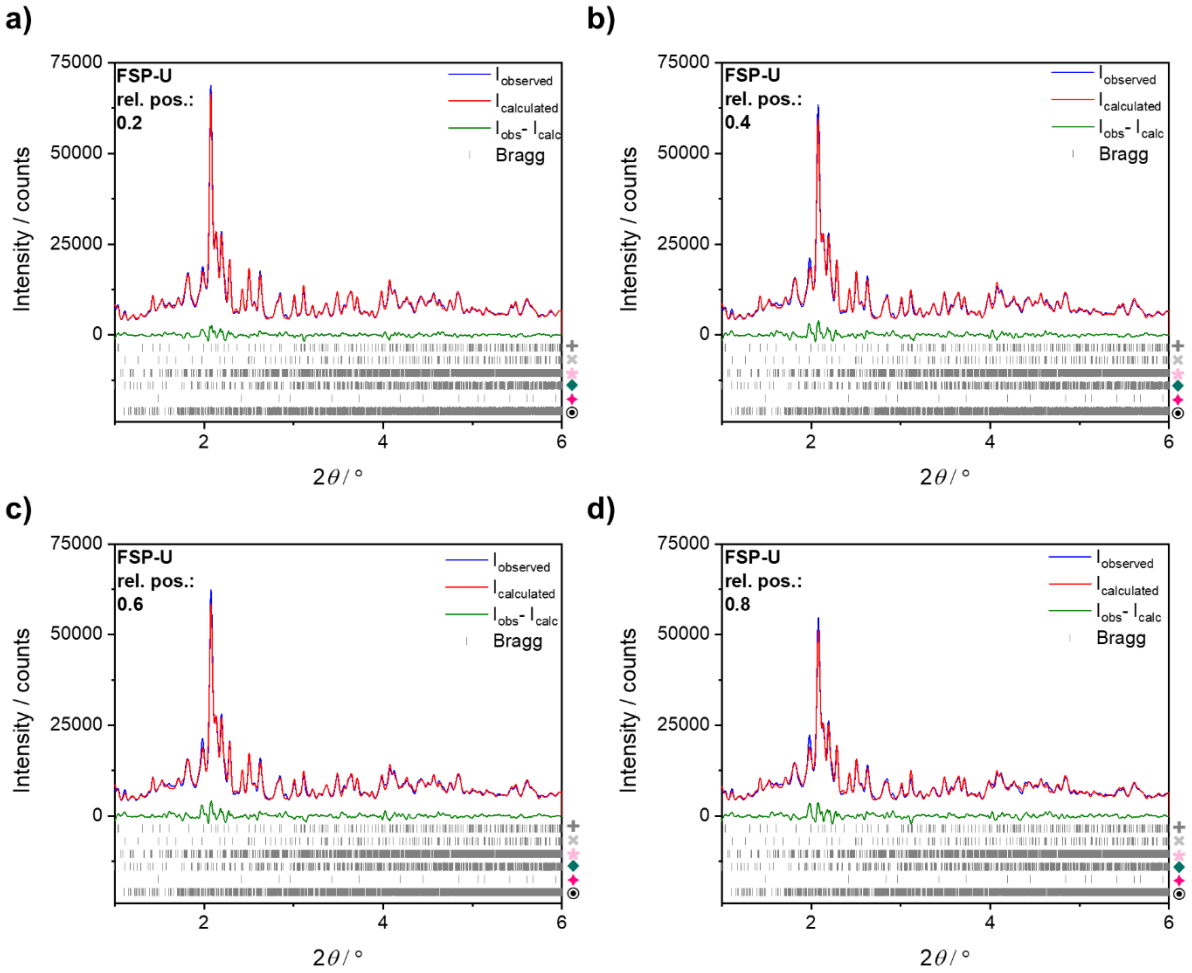


**Figure S10**: Selected Rietveld refinements of FSP-U acquired at different positions along the catalyst bed, referring to relative position 0.2 (a), 0.4 (b), 0.6 (c) and 0.8 (d). Bragg markers refer top down to: $\beta$-$CoMoO_4$ (✚), $\alpha$-$CoMoO_4$ (✖), $Fe_2Mo_3O_{12}$ (✱), $\alpha$-$Bi_2Mo_3O_{12}$ (◆), $Fe_3O_4$ (✦) and $Mo_{18}O_{52}$ (⦿). Fit results are listed in Table S3.

**Table S3:** Selected Rietveld refinements results of FSP-U measured at different positions along the catalyst bed.

| **Results from Rietveld refinement** | **Relative position** | | | |
|---|---|---|---|---|
| | **0.2** | **0.4** | **0.6** | **0.8** |
| ω ($\beta$-$CoMoO_4$) / wt% | 59.2 (6) | 57.8 (7) | 57.2 (7) | 52.0 8) |
| ω ($\alpha$-$CoMoO_4$) / wt% | 3.7 (4) | 4.7 (5) | 4.8 (5) | 5.9 (5) |
| ω ($Fe_2Mo_3O_{12}$) / wt% | 13.7 (5) | 12.9 (6) | 12.9 (7) | 12.7 (8) |
| ω ($\alpha$-$Bi_2Mo_3O_{12}$) / wt% | 11.4 (2) | 10.8 (3) | 10.8 (3) | 10.6 (3) |
| ω ($Fe_3O_4$) / wt% | 5.2 (3) | 5.5 (4) | 5.5 (4) | 6.3 (5) |
| ω ($Mo_{18}O_{52}$) / wt% | 6.9 (4) | 8.4 (5) | 8.7 (6) | 12.5 (6) |
| $R_{exp}$ / % | 1.05 | 1.05 | 1.05 | 1.07 |
| $R_{wp}$ / % | 4.35 | 5.56 | 5.67 | 6.2 |
| $R_p$ / % | 3.42 | 4.32 | 4.41 | 4.84 |
| GOF / % | 4.16 | 5.30 | 5.39 | 5.79 |

# 6 Spatially-resolved *operando* XAS during selective isobutene oxidation

## 6.1 Experimental setup and conditions

An initial spatially-resolved *operando* XAS experiment of FSP-U in selective isobutene oxidation was performed at ROCK beamline at Mo K- and Bi $L_3$-edges in transmission mode (SOLEIL, Saint-Aubin, France). Due to the high X-ray absorption of FSP-U, the catalyst was diluted with α-$Al_2O_3$ in a ratio of 1:3 (m/m), ground, pressed, granulated, and sieved to a fraction of 300-450 µm. Despite the strong dilution, only the acquisition of XAS spectra at Mo K-edge resulted in sufficiently high S/N ratio. 670 mg of the diluted catalyst was placed in a fused silica reactor tube and mounted in the CPR as described in **ESI, section 1**. This resulted in a catalyst bed length of 40.5 mm. First, the catalyst was heated to 180 °C (5 °C/min) in inert atmosphere (He = 100 vol.%, 20 mL/min). Afterwards, the catalyst was heated stepwise (2 °C/min) up to 390 °C under reaction conditions ($He/O_2/C_4H_8/H_2O$ = 70/14/8/8 vol.%, ~ 1 bar). The total flow was set to 20 mL/min in order to probe a weight hourly space velocity (WHSV) of 1.5 $h^{-1}$. Gas lines were heated to 200 °C to prevent water and product condensation. An on-line mass spectrometer (MS, OMNI Star GSD 320, Pfeiffer Vacuum) was used to analyse the gas mixture. After ~3 h of catalyst stabilization, as monitored by MS, the profile was acquired from behind to in front of the catalyst bed with a step size of 5 mm. This resulted in 9 measurement points of concentration, temperature and XAS along the catalyst bed. Precise alignment of the X-ray beam, thermocouple and sampling orifices was ensured by laser alignment in combination with micrometre precision stages.

The XAS data was acquired at 2 Hz with a beam size of 0.5 mm (H) x 0.3 mm (V). A Si(220) monochromator was used at Mo K-edge and a Si(111) monochromator at Bi $L_3$-edge. One acquisition lasted 5 minutes at Mo K-edge and 15 minutes at Bi $L_3$-edge. XAS profiles of the initial and final state of the catalysts (before and after heating) were recorded under He atmosphere at room temperature. Energy calibration, averaging, background subtraction, and normalization were conducted with the beamline software.(19) Further data treatment was performed with the software package IFEFFIT.(20)

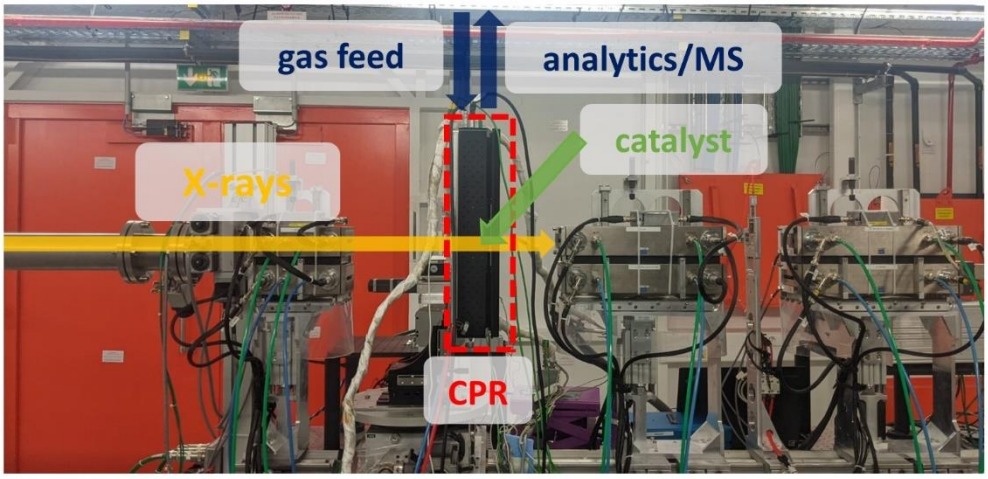


**Figure S11**: Photo of experimental setup for spatially-resolved *operando* XAS experiments at the ROCK beamline (SOLEIL, France).

## 6.2 Results

The XAS results revealed tetrahedrally coordinated Mo along the entire catalyst bed (**Figure S12a**). This was contrary to the XRD profile derived after testing in propylene oxidation, which showed a mixture of octahedral and tetrahedral coordinated Mo along the catalyst bed of FSP-U. In other words, structural changes seemed to occur at different rates during each reaction, with faster structural transformations during more active isobutene oxidation. Hence, tetrahedrally coordinated molybdenum was found to be stable, regardless of the local gas concentration and catalyst temperature. The simultaneously acquired spatially-resolved MS data is shown in **Figure S12b**.

It should be mentioned that solely XAS measurements at Mo K-edge are not sufficient to adequately describe the complex catalyst structure. Hence, future experiments in particular during highly active isobutene oxidation over 4-component systems should further focus on finding experimental compromises in between suitable testing conditions and representative spectroscopic measurements. For example, different diluents than α-$Al_2O_3$ and SiC could be considered, as well as switching to glassy carbon reactor tubes for lower material absorbance during XAS experiments.

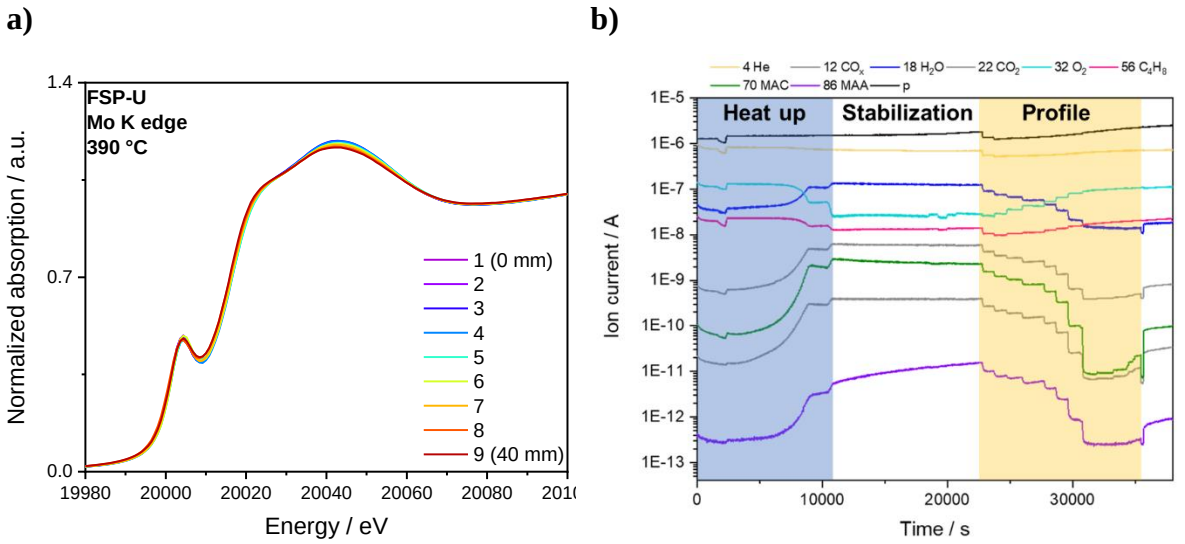


**Figure S12:** XANES spectra at Mo K-edge (a) and MS data (b) acquired simultaneously along the catalyst bed of FSP-U under reaction conditions ($He/O_2/C_4H_8/H_2O$ = 70/14/8/8 vol%; WHSV 1.5 $h^{-1}$) at 390 °C. Catalyst was diluted with $\alpha$-$Al_2O_3$ (1:3).

# References


1. P. Sprenger, M. Stehle, A. Gaur, A. M. Gänzler, D. Gashnikova, W. Kleist, J.-D. Grunwaldt, *ACS Catal.*, 2018,**8**,6462-6475.
2. L. Klag, A. Gaur, M. Stehle, S. Weber, T. L. Sheppard, J.-D. Grunwaldt, *ACS Catal.*, accepted for publication.
3. G. Smith, J. Ibers, *Acta Crystallogr.*, 1965,**19**,269-275.
4. P. Adamski, D. Moszynski, A. Komorowska, M. Nadziejko, A. Sarnecki, A. Albrecht, *Inorg. Chem.*, 2018,**57**,9844-9850.
5. H. Ehrenberg, I. Svoboda, M. Wiesmann, H. Weitzel, *Acta Crystallogr. Sect. C: Cryst. Struct. Commun.*, 1999,**55**,1383-1384.
6. J. P. Picard, G. Baud, J. P. Besse, R. Chevalier, *J. less-common met.*, 1980,99-104.
7. A. Van den Elzen, G. Rieck, *Acta Crystallogr. Sect. B: Struct. Sci.*, 1973,**29**,2433-2436.
8. H.-Y. Chen, A. W. Sleight, *J. Solid State Chem.*, 1986,**63**,70-75.
9. F. Pertlik, J. Zeman, *Fortschr. Mineral.*, 1982,**60**,162-163.
10. G. Malmros, *Acta Chem. Scand.*, 1970,**24**,384-396.
11. A. W. Sleight, B. L. Chamberland, J. F. Weiher, *Inorg. Chem.*, 1968,**7**,1093-1098.
12. M. Rapposch, J. Anderson, E. Kostiner, *Inorg. Chem.*, 1980,**19**,3531-3539.
13. M. Fleet, *Acta Crystallogr. Sect. B: Struct. Sci.*, 1981,**37**,917-920.
14. W. Jeitschko, A. Sleight, W. McClellan, J. Weiher, *Acta Crystallogr. Sect. B: Struct. Sci.*, 1976,**32**,1163-1170.
15. T. Leisegang, A. Levin, J. Walter, D. Meyer, *Cryst. Res. Technol.*, 2005,**40**,95-105.
16. L. Kihlborg, *Arkiv for Kemi*, 1964,**21**,443-460.
17. A. A. Coelho, *J. Appl. Crystallogr.*, 2018,**51**,210-218.
18. D. Balzar. Voigt-function model in diffraction line-broadening analysis. In: R. L. Snyder, H. J. Bunge, J. Fiala, editors. Microstructure Analysis from Diffraction. 10: International Union of Crystallography; 1999. p. 94-126.

19. C. Lesage, E. Devers, C. Legens, G. Fernandes, O. Roudenko, V. Briois, *Catal. Today*, 2019,**336**,63-73.
20. B. Ravel, M. Newville, *J. Synchrotron Radiat.*, 2005,**12**,537-541.